

COUPLED LINE-PROFILE AND CONTINUUM VARIATIONS IN EZ CANIS MAJORIS: IMPLICATIONS FOR THE DRIVING MECHANISM OF GLOBAL WIND STRUCTURES IN WOLF-RAYET WINDS

THIERRY MOREL,¹ NICOLE ST-LOUIS,¹ ANTHONY F. J. MOFFAT,¹ OCTAVIO CARDONA,²
GLORIA KOENIGSBERGER,³ AND GRANT M. HILL⁴

Received 1997 August 20; accepted 1997 December 11

ABSTRACT

EZ CMa is an apparently unusual Wolf-Rayet star of the nitrogen sequence that exhibits strong variations on a period of 3.77 days with coherency lasting typically about 10 cycles. We have used an extensive set of optical spectroscopic observations to investigate a possible link between its line-profile and photometric continuum variability. Despite the strong epoch dependency of the variations, a persistent correlation is found between changes in the wind line profiles (N v $\lambda\lambda 4604, 4620$ in particular) and in continuum flux emanating near the stellar core.

We suggest that these observations give further support to the idea that the physical conditions prevailing in the vicinity of the star's photosphere have a significant impact on the wind structure and that a spatial dependence of these conditions at the base of the outflow induces the formation of azimuthal wind structures in EZ CMa. The epoch-dependent nature of the variability could be related to long-term behavior of corotating magnetic structures, although pulsational instabilities constitute a viable alternative.

Subject headings: stars: individual (EZ Canis Majoris) — stars: mass-loss — stars: Wolf-Rayet

1. INTRODUCTION

Although a few early investigations of spectral variability of OB stars concluded that, in some cases, the outflow is probably far from being spherically symmetric or steady (e.g., Ebbets 1982; Grady, Snow, & Timothy 1983), it is only recently that a global view of the phenomenon and a comprehensive picture have begun to emerge (e.g., Howarth, Prinja, & Massa 1995; Massa, Prinja, & Fullerton 1995; Prinja, Massa, & Fullerton 1995; Kaper et al. 1996, 1997; Kaufer et al. 1996a, 1996b; Reid & Howarth 1996; Prinja, Fullerton, & Crowther 1996). In the light of these studies, some fundamental conclusions can be drawn: (1) the time-scale of the wind line-profile variations (LPVs) is generally compatible with the stellar rotation period, which could imply that the variability is induced by the rotational modulation of a large-scale inhomogeneous outflow and (2) there is some evidence for a direct link between photospheric and wind activity, pointing to mechanisms such as photospheric magnetic structures or (non)radial pulsations to trigger the formation of such aspherical winds.

Hydrodynamical simulations by Cranmer & Owocki (1996) have indeed demonstrated that an azimuthal dependence of the radiative flux emanating from the photosphere (due, e.g., to pulsations; Fullerton, Gies, & Bolton 1996) can lead to a structured wind with streams curved by the stellar rotation outflowing at different speeds from the “active” regions. In essence, an analogy can be made with the “corotating interacting regions,” which are characteristic

features of the solar corona (Hundhausen 1972; Gosling 1996). The ability of this conceptually simple model to reproduce the behavior of the “discrete absorption components” (DACs) moving shortward in the P Cygni absorption components of the UV resonance lines of most O stars raises the possibility that the development of such structures could be widespread among the OB-star population (Cranmer & Owocki 1996; Owocki, Cranmer, & Fullerton 1995). Their possible occurrence in hot-star winds was first discussed from a qualitative viewpoint by Mullan (1984, 1986) and Harmanec (1991).

The existence of globally aspherical outflows in Wolf-Rayet (W-R) stars is currently a matter of debate, although the lack of depolarization (compared to continuum polarization) across the emission lines of the majority of these objects suggests that in first approximation the outflows are spherically symmetric (Schulte-Ladbeck 1995; Harries, Hillier, & Howarth 1998). However, although most of the spectral and photometric variability displayed by single W-R stars can generally be ascribed to the strong stochastic inhomogeneities at relatively small scales, which may be ubiquitous in all radiatively driven outflows (Moffat & Robert 1992; Eversberg, Lépine, & Moffat 1998), a small number of remarkable W-R stars present systematic, large-scale spectral variations, which are probably induced by an additional phenomenon, possibly the same that generates DACs in O-star winds (Lépine, Moffat, & Henriksen 1996). In addition, these W-R stars are among the few that present strong, variable depolarization in their line profiles (see, e.g., Schulte-Ladbeck et al. 1992). Hence, a global departure from isotropic outflow could constitute a natural explanation for these observed large-scale changes. Furthermore, recent intensive photometric and spectroscopic monitoring of WN8 stars has shown that physical processes operating in the deepest (“invisible”) layers of their winds could be, as in OB stars, responsible for their intrinsically high level of variability (Marchenko et al. 1998).

What might turn out to be the “prototype” of this class is the WN5 (WN4 in the new three-dimensional system of Smith, Shara, & Moffat 1996) star EZ CMa (W-R 6, HD

¹ Département de Physique, Université de Montréal, C.P. 6128, Succ. Centre-Ville, Montréal, Québec, Canada, H3C 3J7, and Observatoire du Mont Mégantic; morel@astro.umontreal.ca, stlouis@astro.umontreal.ca, moffat@astro.umontreal.ca.

² Instituto Nacional de Astrofísica, Óptica y Electrónica, Apdo. Postal 51, Puebla, Pue. 72000, Mexico; ocardona@inaoep.mx.

³ Instituto de Astronomía, UNAM, Apdo. Postal 70-264, Mexico D.F. 04510, Mexico; gloria@astroscu.unam.mx.

⁴ National Research Council, Herzberg Institute of Astrophysics, Dominion Astrophysical Observatory, 5071 West Saanich Road, Victoria, British Columbia, Canada V8X 4M6; present address: McDonald Observatory, HET, P. O. Box 1337, Fort Davis, TX; grant@astro.as.utexas.edu.

TABLE 1
JOURNAL OF SPECTROSCOPIC OBSERVATIONS

SPECTROSCOPY								PHOTOMETRY		
EPOCH	Date	HJD - 2,440,000	Observatory ^a	Number of Spectra	Spectral Coverage (Å)	Reciprocal Dispersion (Å pix ⁻¹)	S/N	HJD - 2,440,000	Filter	Reference
I.....	91 Jan	8280–8291	SPM	283	4435–5020	1.04	~150	8281–8294	y	1
II.....	91 Oct	8550–8563	UTSO	11	3750–4575	1.60	~100	"	y	1
				11	4200–5025	1.60				
III ^b	92 Jan	8642–8655	UTSO	21	4550–5050	0.97	~130	"	y	1
IV.....	92 Oct	8900–8917	UTSO	11	3620–4540	2.16	~225	8918–8931 ^c	y	1
				11	4165–5210	2.16				
V.....	93 Mar	9046–9053	UTSO	8	3640–4505	2.16	~230	9038–9089	5140 Å	2
				8	4110–4975	2.16				
				8	5115–5980	2.16				
VI.....	94 Mar	9428–9445	UTSO	18	4000–4820	1.60	~220	9383–9450	U, B, V	3

^a SPM: San Pedro Mártir Observatory 2.1 m; UTSO: University of Toronto Southern Observatory 0.6 m.

^b Simultaneous *IUE* spectra were collected during the period HJD 2,448,643–2,448,649 (St-Louis et al. 1998).

^c For the correction of the continuum variability in the spectra, this light curve was interpolated.

REFERENCES.—(1) Duijsens et al. 1996; (2) Antokhin et al. 1994; (3) this study.

50896), which exhibits an unusual and striking periodic variability (with $\mathcal{P} = 3.77$ days) in spectrophotometry (Firmani et al. 1980), continuum photometry (Antokhin et al. 1994), and polarimetry (Robert et al. 1992). Because of the periodicity of the changes and the lack of detection of a normal stellar companion, some authors have suggested that this W-R star harbors a compact companion (Ebbets 1979; Firmani et al. 1980). This appealing conclusion has, however, often been questioned on various grounds in the literature (e.g., Stevens & Willis 1988; Willis et al. 1989; St-Louis et al. 1993). The controversial nature of this object is illustrated by the fact that models including an orbiting neutron star companion or variability intrinsic to the wind itself have both been claimed to give an acceptable fit to the spectroscopic data (Matthews et al. 1992b; Koenigsberger 1995). Recently, further arguments were presented against the possible duplicity of this object (Morel, St-Louis, & Marchenko 1997; hereafter, MSM); rather, it has been suggested that the unique 3.77 day period, known for a long time in all modes of observation, is induced by the rotational modulation of the structured W-R envelope. This conclusion was also reached by St-Louis et al. (1995, 1998) from an analysis of spectral variability in the ultraviolet. In view of the tight correlation found between the photometric and spectroscopic changes, the triggering of the wind variability by some process (probably of magnetic or pulsational origin) operating near the stellar core was also proposed.

In this paper, we present an extensive set of optical spectroscopic observations spread over 3 years (1991–1994). In view of the well-known epoch-dependent nature of the spectroscopic and photometric variability of EZ CMa (St-Louis et al. 1993, 1995; Duijsens et al. 1996), the main goal of this study is to investigate the relationship between the level of continuum flux emerging from the inner stellar wind, closest to the stellar core, and the spectroscopic changes, on a much longer timescale than done by MSM. To achieve this, we will discuss the pattern of spectral variability at different epochs in connection with (quasi-)simultaneously acquired archival, as well as new, optical light curves.

Following a description of the spectroscopic data and of their reduction (§ 2.1), we will present new *UBV* light curves in § 2.2. The LPVs will be discussed in § 3, while § 4.1 will emphasize their direct link with the photometric variations.

Finally, the cause of a nonisotropic base outflow will be explored in § 4.2.

2. OBSERVATIONS

2.1. Spectroscopy

We observed EZ CMa on several occasions between 1991 and 1994. The journal of observations is presented in Table 1, which lists successively the epoch number, the date of the spectroscopic observations, the interval of the observations in Heliocentric Julian Days, the observatory name, the number of spectra obtained, the selected spectral domain, the reciprocal dispersion of the spectra, and the typical signal-to-noise ratio (S/N) in the continuum. The last three columns of Table 1 indicate which data set was used for the correction of the continuum variability (see below). Part of this large data set (epochs I and III) has already been briefly discussed by St-Louis (1994). A detailed description of the epoch I data set is presented by Cardona et al. (1998).

Standard reduction procedures (i.e., bias subtraction, flat-fielding, removal of cosmic-ray events, background subtraction, extraction of the spectra, and wavelength calibration) were carried out using IRAF⁵ software packages. For the rectification of the spectra with respect to the continuum, a third- to sixth-order Legendre polynomial was fitted to carefully selected line-free regions. For the last three epochs, consecutive exposures obtained over short periods of time (generally a few minutes) were combined, leading to a significantly higher S/N in the net spectrum (Table 1). No short-term variations were detected from one exposure to another. Note that the timescales involved are too short to detect any significant motion of “blobs.”

In order to remove the contribution to the line variability induced by the rectification process combined with the changing continuum flux, we applied the method described in MSM, i.e., we multiplied each rectified spectrum corresponding to a given phase ϕ by $10^{-0.4[m(\phi) - m(\min)]}$, where $m(\phi)$ and $m(\min)$ are the magnitudes at phase ϕ (the light

⁵ IRAF is distributed by the National Optical Astronomy Observatories, operated by the Association of Universities for Research in Astronomy, Inc., under cooperative agreement with the National Science Foundation.

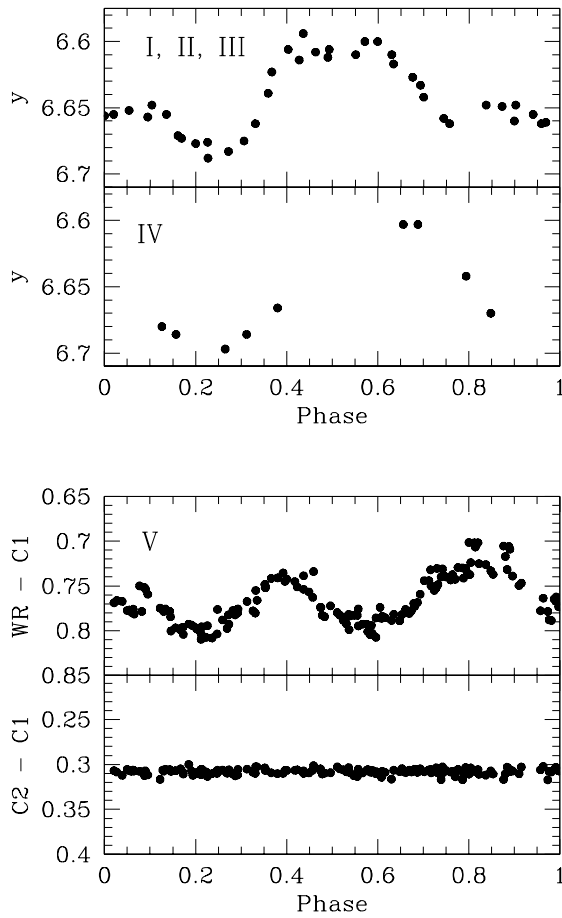


FIG. 1.—*Top*: The y -magnitudes of EZ CMa for the periods HJD 2,448,281–2,448,294 (epochs I, II, and III) and HJD 2,448,918–2,448,931 (epoch IV) (Duijsens et al. 1996). *Bottom*: Narrowband light curve of EZ CMa for the period HJD 2,449,038–2,449,089 (epoch V) (Antokhin et al. 1994); *upper*, differential light curve of EZ CMa; *lower*, differential light curve of the comparison stars c1 and c2. The phases, as everywhere in this paper, are calculated according to the ephemeris of Lamontagne, Moffat, & Lamarre (1986). These figures are adapted from Duijsens et al. (1996) and Antokhin et al. (1994), with permission.

curves were binned to 0.05 phase resolution) and at minimum light, respectively. The constant continuum level in the rectified spectrum was subtracted before this procedure and added back in afterward. Because of the epoch-dependent nature of the photometric changes, the spectra were corrected (when possible) by quasi-simultaneously acquired photometric data. These data were taken from the literature (see Table 1) and were supplemented by new broadband light curves obtained in 1994 by the Automatic Photometric Telescope (see § 2.2). Since we will continually refer to the light curves presented by Duijsens et al. (1996) and Antokhin et al. (1994) throughout this paper, these are reproduced for the sake of clarity in Figure 1. Note that the panels give calibrated (top) and differential magnitudes (bottom). Unfortunately, the spectroscopic and photometric data do not coincide (or even overlap) in some cases. This problem is most severe for the spectra from epochs II and III during which, to our knowledge, no optical light curves were recorded. However, as pointed out by St-Louis et al. (1998), the UV continuum variations observed during epoch III are very similar to the optical continuum variations observed during epoch I (Fig. 1, top). Because the UV

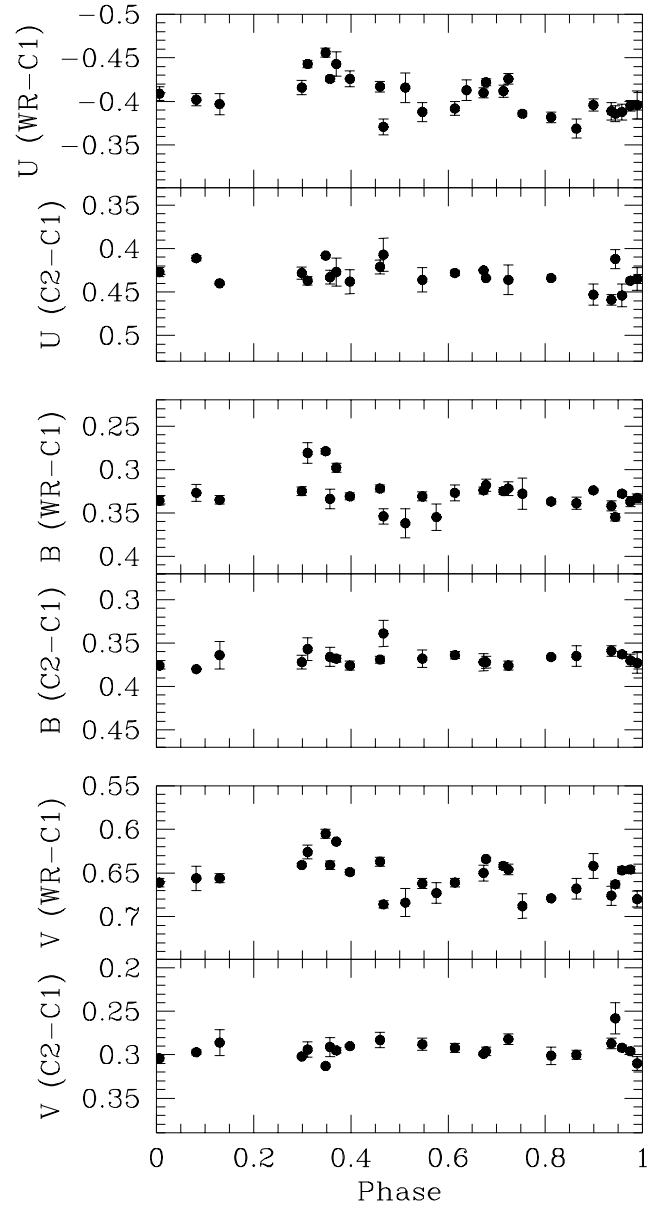


FIG. 2.—*UVB* light curves of EZ CMa for the period HJD 2,449,383–2,449,450 (epoch VI). *Upper panels*: Differential light curve of EZ CMa. *Lower panels*: Differential light curve of the comparison stars c1 and c2. The error bars (2σ) correspond to the internal standard deviations (see Table 2).

and optical continuum flux are strictly related (MSM), this light curve was adopted for epoch III, as well as for epoch II. For the other cases, the desynchronization never exceeds two weeks (epoch IV), an interval that is sufficiently short to expect no gross changes in the light curve shape or amplitude.

2.2. Photometry

New photometric data were gained in order to help establish a reference for epoch VI. EZ CMa was monitored during the period 1994 January 31–April 8 using Johnson *UBV* filters with one of the 0.25 m automatic telescopes on Mount Hopkins (Young et al. 1991). HD 50853 and HD 50711 were used as comparison (c1) and check (c2) stars, respectively. The following sequence of 10 s integrations in each filter was used to derive the differential magnitudes

TABLE 2
DIFFERENTIAL *UBV* MAGNITUDES OF EZ CMA IN 1994^a

HJD - 2,440,000	ϕ	<i>U</i> (mag)		<i>B</i> (mag)		<i>V</i> (mag)	
		W-R - c1	c2 - c1	W-R - c1	c2 - c1	W-R - c1	c2 - c1
9383.7621	0.714	-0.412 (0.007)		0.325 (0.004)		0.642 (0.004)	
9384.7424	0.975	-0.395 (0.006)	0.437 (0.001)	0.337 (0.006)	0.370 (0.007)	0.646 (0.004)	0.296 (0.002)
9386.7674	0.512	-0.416 (0.017)		0.362 (0.017)		0.684 (0.016)	
9389.7288	0.299	-0.416 (0.008)	0.428 (0.007)	0.325 (0.005)	0.372 (0.008)	0.641 (0.002)	0.302 (0.001)
9393.7138	0.357	-0.426 (0.003)	0.433 (0.008)	0.334 (0.011)	0.366 (0.011)	0.641 (0.005)	0.291 (0.011)
9394.7733	0.638	-0.413 (0.012)					
9398.6893	0.678	-0.422 (0.004)	0.434 (0.001)	0.318 (0.007)	0.372 (0.007)	0.634 (0.002)	0.296 (0.005)
9399.6918	0.944	-0.386 (0.009)	0.412 (0.011)	0.355 (0.004)		0.663 (0.004)	0.258 (0.018)
9403.6895	0.006	-0.409 (0.008)	0.427 (0.005)	0.336 (0.005)	0.376 (0.003)	0.661 (0.005)	0.304 (0.003)
9406.7253	0.812	-0.382 (0.006)	0.434 (0.001)	0.337 (0.003)	0.366 (0.002)	0.679 (0.001)	0.301 (0.010)
9410.6881	0.864	-0.369 (0.011)		0.339 (0.007)	0.365 (0.012)	0.668 (0.012)	0.300 (0.005)
9411.6878	0.130	-0.397 (0.012)	0.440 (0.002)	0.335 (0.005)	0.364 (0.016)	0.656 (0.005)	0.286 (0.015)
9412.6970	0.398	-0.426 (0.009)	0.438 (0.014)	0.331 (0.004)	0.376 (0.005)	0.649 (0.003)	0.290 (0.002)
9416.6966	0.460	-0.417 (0.006)	0.421 (0.008)	0.322 (0.004)	0.369 (0.004)	0.637 (0.005)	0.283 (0.009)
9417.6934	0.724	-0.426 (0.006)	0.436 (0.017)	0.322 (0.008)	0.376 (0.005)	0.646 (0.006)	0.282 (0.006)
9418.6903	0.989	-0.396 (0.016)	0.435 (0.013)	0.333 (0.005)	0.373 (0.012)	0.680 (0.009)	0.310 (0.008)
9423.6696	0.311	-0.443 (0.004)	0.437 (0.005)	0.281 (0.012)	0.357 (0.013)	0.626 (0.008)	0.294 (0.009)
9424.6679	0.576			0.355 (0.015)		0.673 (0.012)	
9427.6584	0.370	-0.443 (0.014)	0.427 (0.016)	0.298 (0.005)	0.368 (0.004)	0.614 (0.000)	0.295 (0.003)
9429.6499	0.899	-0.396 (0.007)	0.453 (0.012)	0.324 (0.002)		0.642 (0.014)	
9433.6380	0.958	-0.388 (0.009)	0.454 (0.013)	0.328 (0.003)	0.363 (0.003)	0.647 (0.004)	0.292 (0.003)
9436.6308	0.753	-0.386 (0.003)		0.328 (0.018)		0.688 (0.014)	
9439.6236	0.547	-0.388 (0.011)	0.436 (0.014)	0.331 (0.005)	0.368 (0.010)	0.662 (0.006)	0.288 (0.007)
9441.6382	0.082	-0.402 (0.007)	0.411 (0.003)	0.327 (0.010)	0.380 (0.009)	0.656 (0.014)	0.297 (0.003)
9442.6387	0.348	-0.456 (0.005)	0.408 (0.000)	0.279 (0.003)		0.605 (0.005)	0.313 (0.001)
9443.6389	0.614	-0.392 (0.008)	0.428 (0.003)	0.327 (0.009)	0.364 (0.004)	0.661 (0.005)	0.292 (0.005)
9447.6269	0.673	-0.410 (0.006)	0.425 (0.000)	0.324 (0.004)	0.372 (0.010)	0.650 (0.009)	0.299 (0.002)
9448.6195	0.936	-0.389 (0.010)	0.459 (0.006)	0.342 (0.006)	0.359 (0.006)	0.676 (0.011)	0.287 (0.006)
9450.6203	0.467	-0.371 (0.009)	0.407 (0.019)	0.354 (0.009)	0.339 (0.015)	0.686 (0.004)	

^a The internal standard deviation of the data is given in brackets. The empty cells in the table are due to rejection of the data when this number exceeds 0.02 mag (Young et al. 1991).

listed in Table 2: c2, sky, c1, W-R, c1, W-R, c1, W-R, c1, sky, c2. The internal standard deviations are also quoted in Table 2. The mean external standard deviations of the (c2 - c1) data are 0.006, 0.004, and 0.005 mag for the *U*, *B*, and *V* filters, respectively. These values are typical of the accuracy achieved by this robotic telescope (Strassmeier & Hall 1988). The flux in each of the three filters suffers from various line emission contributions (Duijsens et al. 1996): 22% (*U*), 30% (*B*), and 11% (*V*). The data are plotted as a function of phase in Figure 2. The phases, as everywhere in this paper, are calculated according to the ephemeris of Lamontagne, Moffat, & Lamarre (1986).

3. RESULTS

3.1. An Overview of the LPVs: He II $\lambda 4686$

In order to display the LPVs as conspicuously as possible and because the variations were strictly repeatable from one cycle to another during our observing runs (which covered at most five cycles; Table 1), we have grouped the individual spectra for a given epoch into 0.05 phase resolution bins. Also, we have chosen to illustrate the LPVs by means of the strong He II $\lambda 4686$ emission line. As will be shown below (§ 3.2), this transition exhibits variations that are very much representative of those affecting the majority of the other spectral lines present in the spectrum of EZ CMA. We compare the individual binned spectra with the corresponding mean spectrum of each epoch in Figures 3a–3c for the spectral range encompassing He II $\lambda 4686$. Remarkable phase-dependent changes in the line-peak morphology are observed. Also, this data set nicely exhibits the well-known

epoch dependency (on a typical timescale of weeks to months) displayed by this star. At this point, we emphasize that some caution must be taken when making a direct comparison between different epochs. Because of the period uncertainty (accurate, at best, to the third decimal place), substantial phase shifts can occur if the observing runs are separated by some years, as is the case here. Even allowing for such potential slippage, however, there is little doubt that the pattern of variability has dramatically changed between epochs I and II (secured as little as only ~ 70 cycles apart; Table 1). In addition to the line-peak variability, significant smaller changes (see § 3.4) are also present in the line wings out to at least $v \sim \pm 2500 \text{ km s}^{-1}$.

3.2. Similarities in the Pattern of Variability for Different Lines

We present in Figures 4a–4b gray-scale plots of the residual deviations from the mean spectrum of He II $\lambda 4686$ and He II $\lambda 4859$ from epoch I, for which we have obtained the best phase coverage. These residual spectra were binned to 0.02 phase resolution and are arranged as a function of phase in the upper portion of each panel. As illustrated, these two He II transitions share the same pattern of variability, with only a small phase lag of the stronger He II $\lambda 4686$ line behind He II $\lambda 4859$. This similarity between the LPVs affecting all the He II transitions is also observed for the other epochs and seems to constitute a definite feature of the wind variability of EZ CMA (see MSM).

Figure 4c displays the gray-scale plot of N V $\lambda 4945$. This transition is of interest since it is formed relatively close to the stellar core, contrary to other transitions such as He II

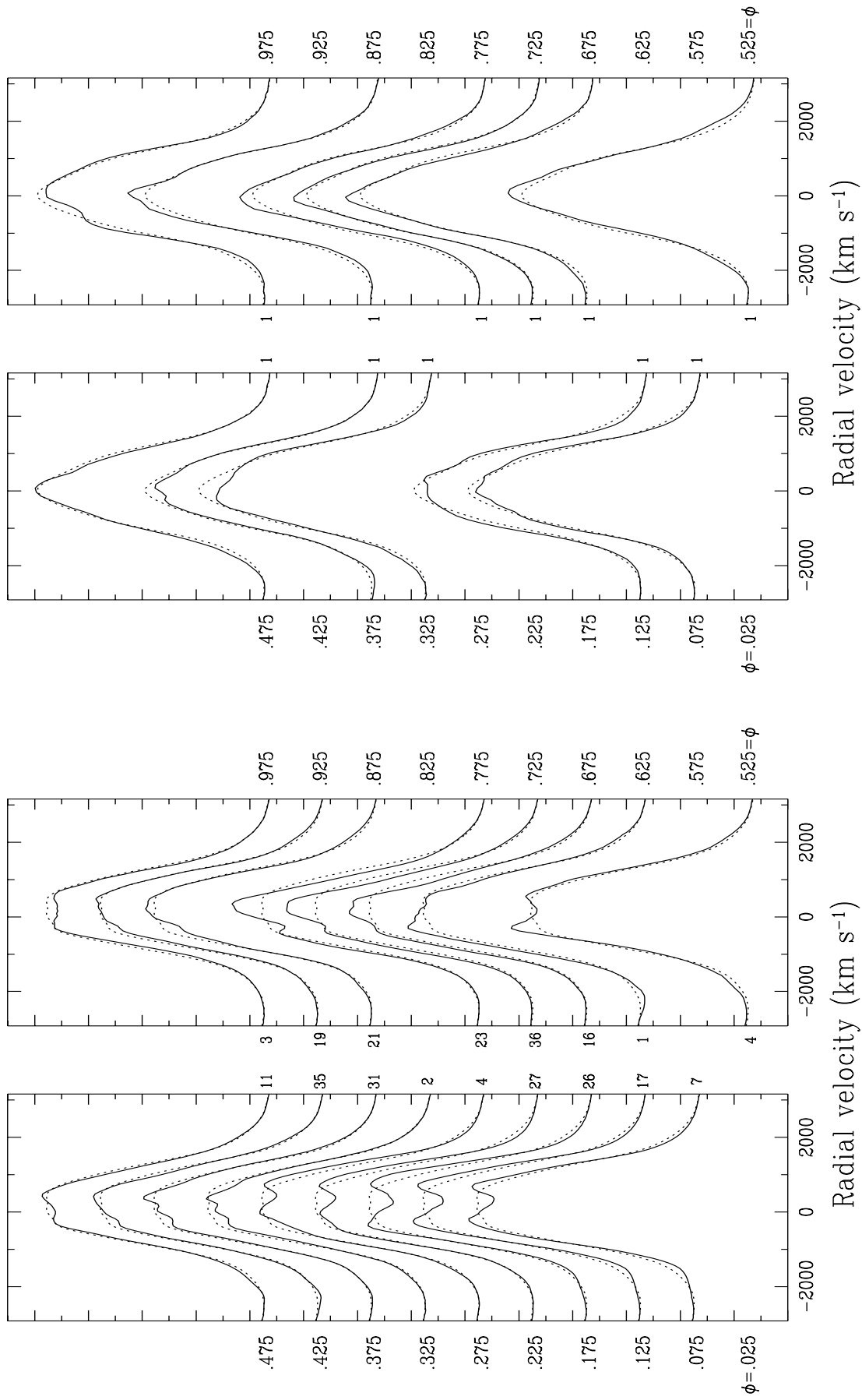


FIG. 3a

FIG. 3.—Time series of He II $\lambda 4686$ for the six different epochs: (a) epoch I (left) and epoch II (right); (b) epoch III (left) and epoch IV (right); (c) epoch V (left) and epoch VI (right). The rectified spectra were binned to 0.05 phase resolution (the number of spectra averaged to form the corresponding binned spectrum is indicated between the two panels of each figure). The mean phases are also indicated on both sides of these plots. The mean of the binned spectra is overlaid as a dashed line for each epoch. The projected velocities, as everywhere in this paper, are heliocentric and refer to the laboratory rest wavelength.

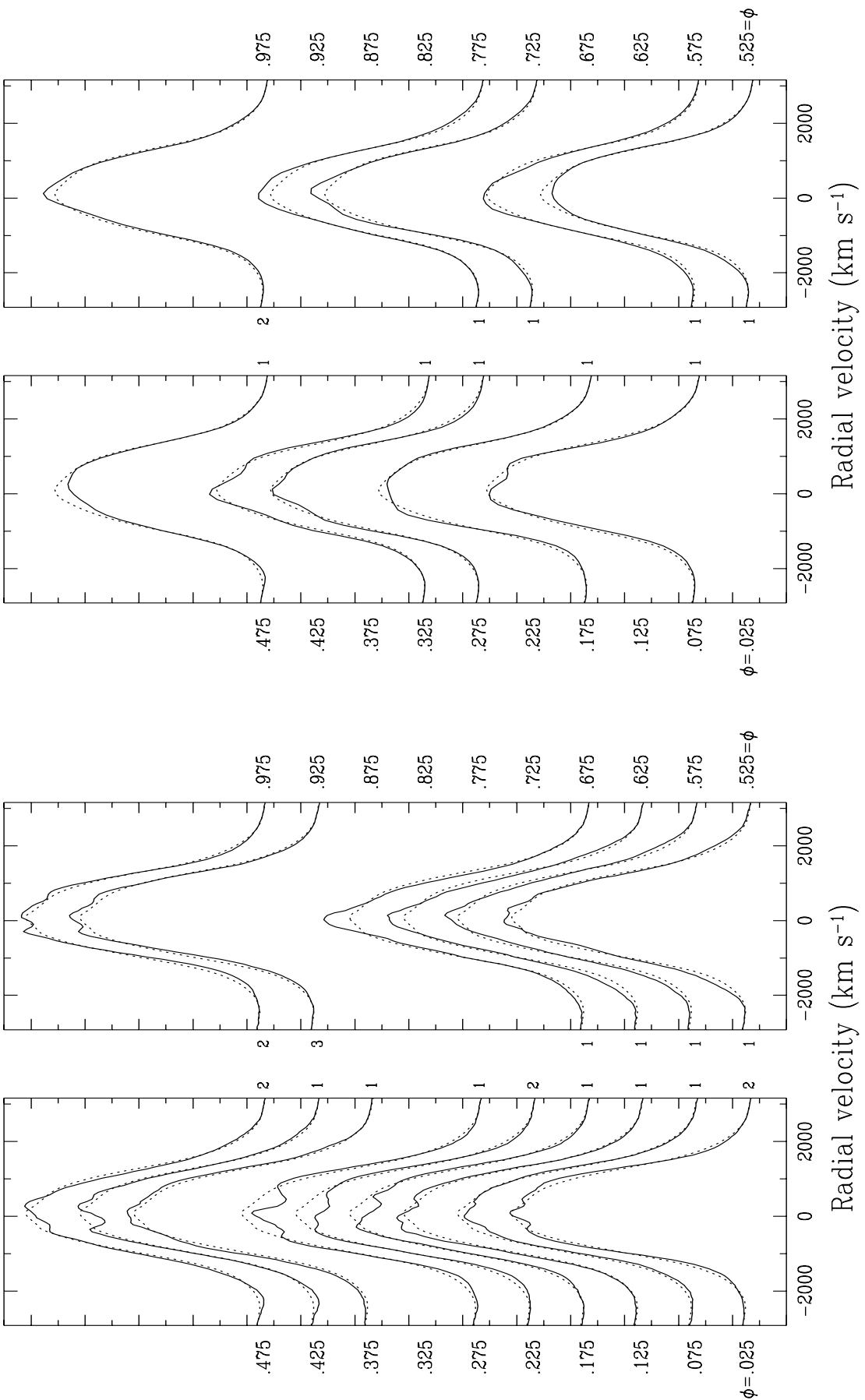


FIG. 3b

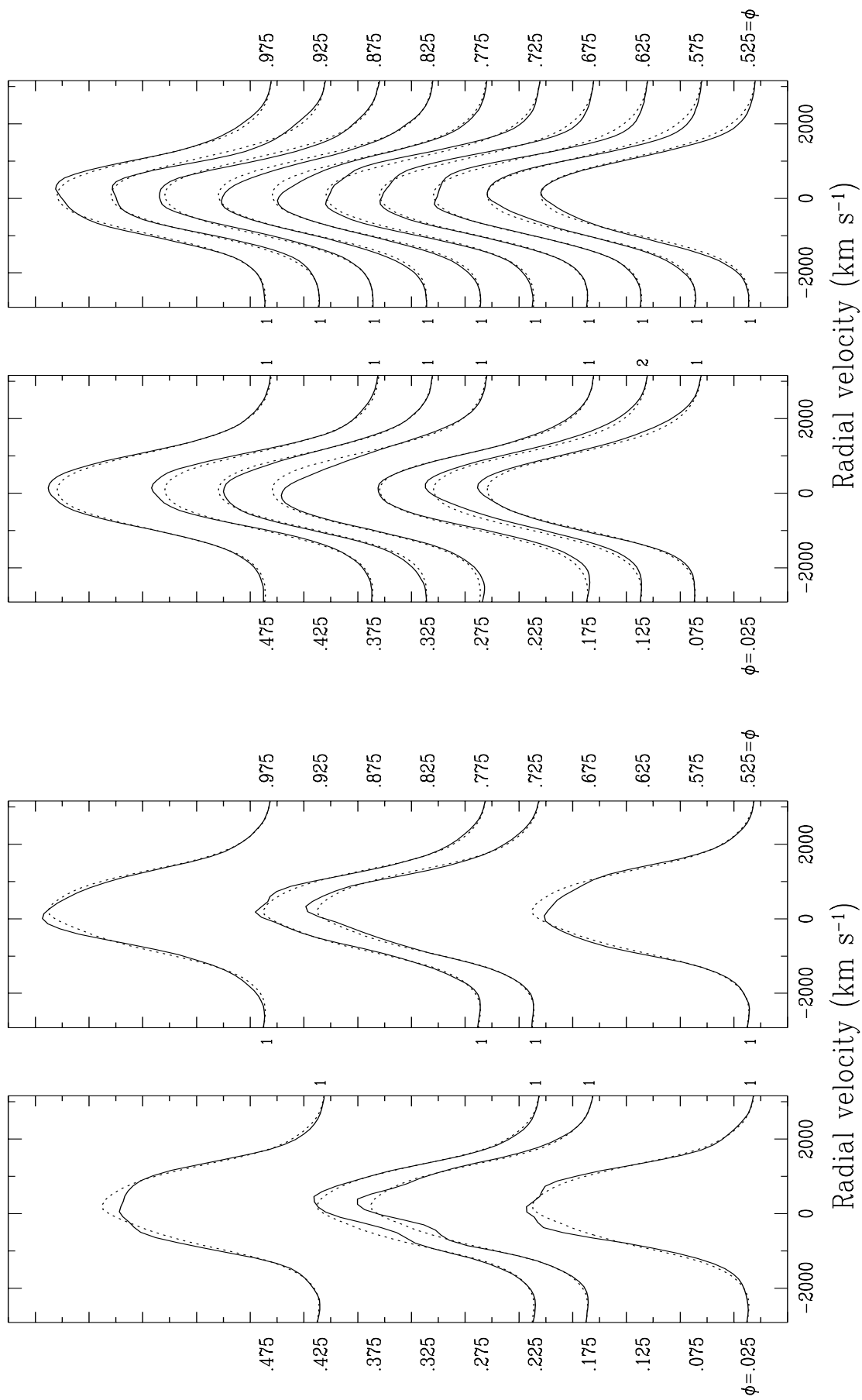


FIG. 3c

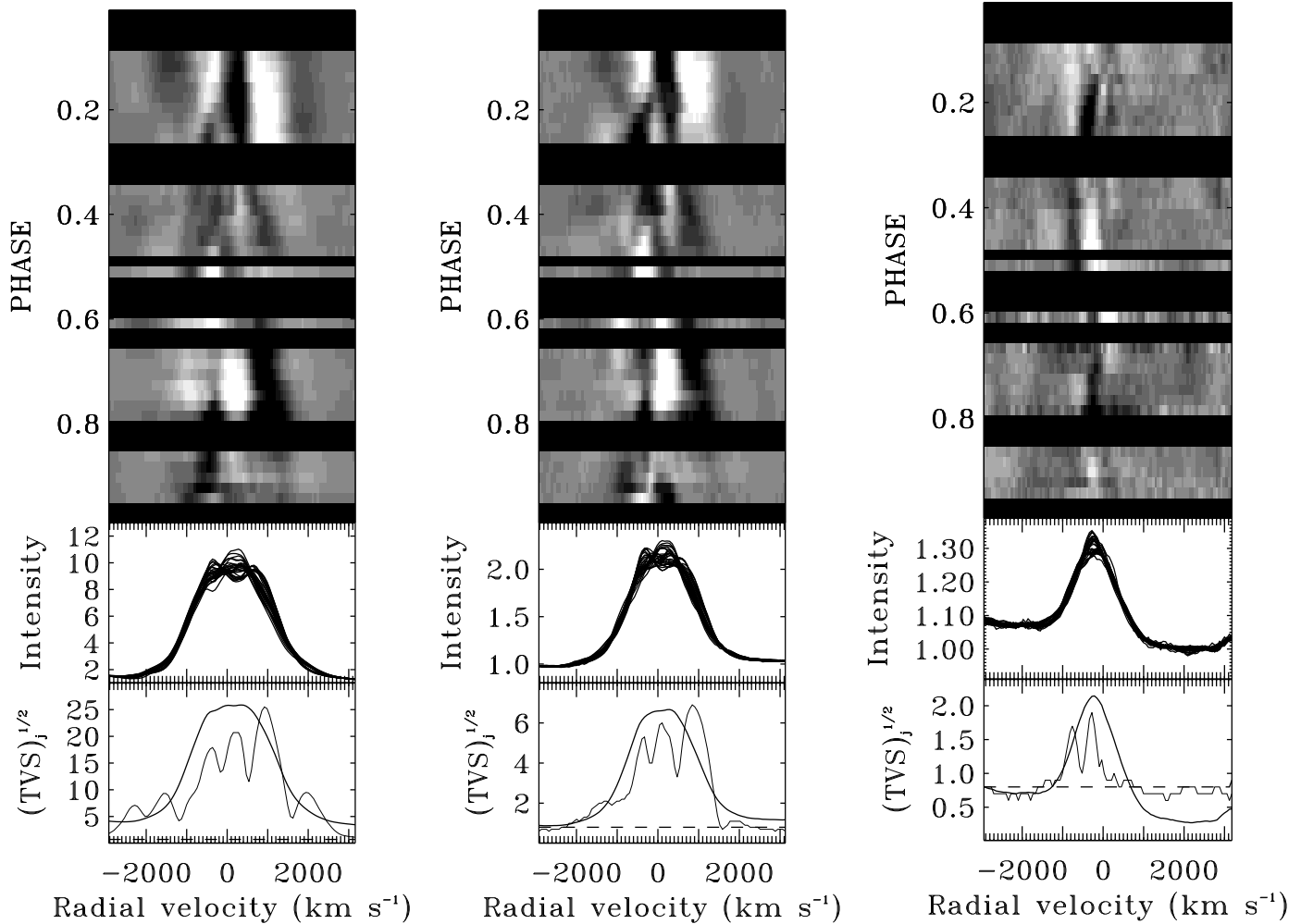


FIG. 4a

FIG. 4b

FIG. 4c

FIG. 4.—Gray-scale plots of the time series of the residuals of (a) He II $\lambda 4686$ (range: -0.7 to 0.7), (b) He II $\lambda 4859$ (range: -0.1 to 0.1), and (c) N V $\lambda 4945$ (range: -0.03 to 0.03) for epoch I. These residuals (the mean profile of the epoch subtracted from the individual profiles) were binned to 0.02 phase resolution. Excess emission components appear brighter in these plots. The middle portion of each panel presents the superposition of the different rectified profiles. The values of $(TVS)_j^{1/2}$ (§ 3.4) and the mean profile (in arbitrary units) are displayed in the lower portion of each panel. The horizontal dashed line indicates the 99.0% variability detection threshold.

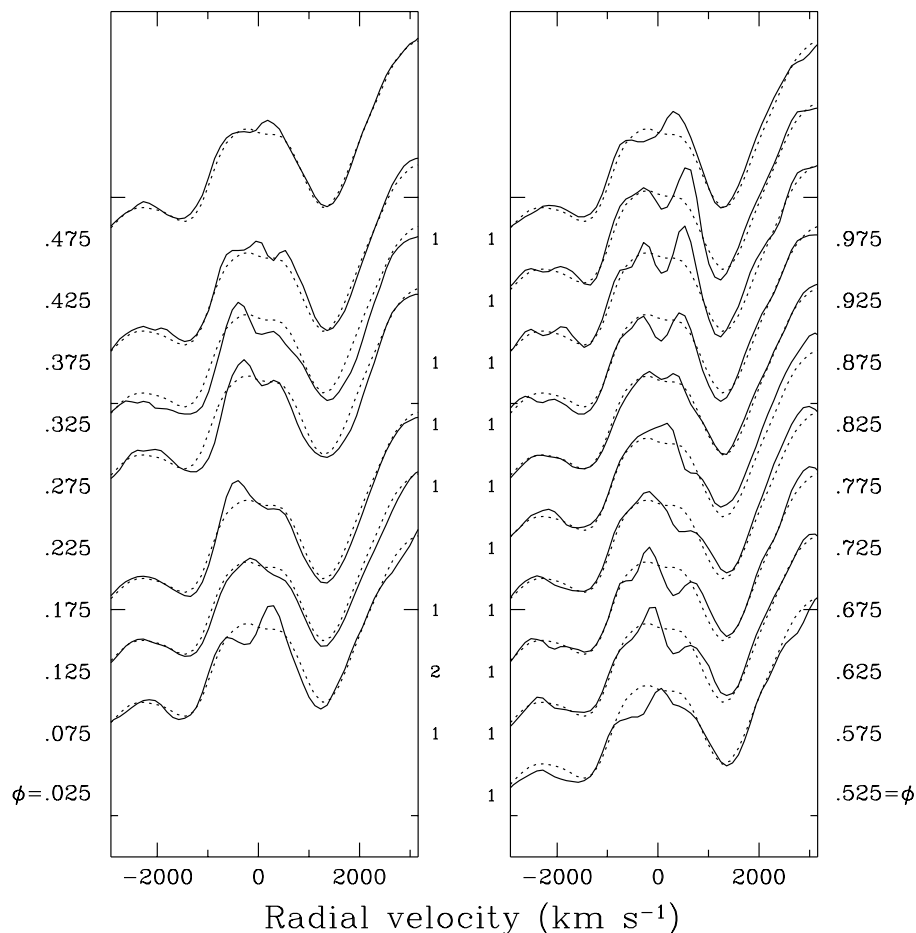
$\lambda 4686$. The bulk of emission in the nitrogen and helium lines arises at about 2.5 and 12 stellar core radii, respectively (P. A. Crowther 1995, private communication). Although significant (see § 3.4), the LPVs in this line are very subtle, even accounting for its weakness (MSM), and cannot easily be linked to those in the helium transitions discussed above. However, N V $\lambda 4945$ shares with the He II lines the peculiarity of also exhibiting cyclical changes according to the 3.77 day period (the variations are coherent over the three cycles covered by the observations). This suggests that the variability is rooted to processes operating in the deep layers of the wind. There is also a hint in Figure 4c that the structures in N V $\lambda 4945$ are seen earlier in phase than those in the He II lines (as N IV $\lambda 4058$ in 1995; MSM).

The relatively good phase coverage achieved during epoch VI allows one to characterize fairly well the N IV $\lambda 4058$ LPVs (Fig. 5). As can be seen, this transition is extremely sensitive to time-dependent wind conditions. Owing to the modest changes in the line-profile morphology of He II $\lambda 4686$ (Fig. 3c, right), it is not clear from this data set whether these N IV LPVs are (as found by MSM)

similar to the variations in the He II line. Two states within the cycle can be defined: one with a strongly enhanced blue peak ($\phi \sim 0.175$ – 0.325 and $\phi \sim 0.575$ – 0.725) and red peak ($\phi \sim 0.875$ – 0.075), respectively. Note the abrupt ($\Delta\phi = 0.1$; ~ 9 hr) shift between these two “states” at $\phi \sim 0.125$.

3.3. Correlated Continuum and Line-Profile Variations

In order to search for a possible correlation between the line profile and the photometric (continuum) variations, we have calculated the Spearman rank-order correlation coefficient (Press et al. 1992) between the line intensity at a given wavelength and the continuum flux level. The binned spectra of Figure 3 were used in this procedure, along with the continuum flux at the corresponding phase, which was determined by binning the light curves to 0.05 phase resolution. For epoch VI, we have averaged the U , B , V light curves displayed in Figure 2. We stress that the rectified spectra used in this procedure have been corrected for the effect of the continuum flux variability (§ 2.1); that is to say, the line-profile variations reflect the genuine changes in the line emissivity at any given projected velocity. The

FIG. 5.—Time series of N IV $\lambda 4058$ for epoch VI

results for each epoch (we have excluded epoch IV because of the poor phase coverage of the light curve [Fig. 1, *top*] but included the data from 1995 January [MSM]) are displayed in Figure 6 for the spectral region encompassing He II $\lambda 4686$. The horizontal lines indicate the 99.0% and 99.9% confidence levels for a significant (anti)correlation. Although this investigation yields negative results at these levels for epochs II and V, the line intensity in some velocity regions is occasionally directly linked to the level of continuum flux for epochs I, III, and VI, as well as for the data acquired in 1995 January. For example, a positive correlation is observed for epochs I and III and in 1995 January between the line intensity and the level of continuum flux at $v \sim +2000 \text{ km s}^{-1}$.

This correlation is particularly remarkable for epoch III, for which the line intensity at -1600 , $+300$, and $+2200 \text{ km s}^{-1}$ is strongly ($>99.9\%$) positively correlated with the continuum flux level, whereas it is anticorrelated at $+1200 \text{ km s}^{-1}$.⁶ This result is reminiscent of the anticorrelated variations at the same blueward and redward projected outflow velocity observed in the H α line of the O supergiant HD 152408 by Prinja & Fullerton (1994). These (anti)correlations observed during epoch III in EZ CMa are probably a result of the oscillation between rather flat-topped and triangular profiles (Fig. 3*b*, *left*) observed at

minimum and maximum continuum flux, respectively ($\phi \sim 0.2$ and $\phi \sim 0.6$, respectively; see Fig. 1, *top*). Similar phase-dependent changes in the line-profile “morphology” were also observed in 1994 (Georgiev & Ivanov 1995). The correlation function is displayed in Figure 7 for the entire spectral domain covered during epoch III. Clearly, the phenomenon described above is by no means restricted to He II $\lambda 4686$; a very similar correlation pattern is also observed for the other transitions, including N V $\lambda 4945$. In particular, the correlation across the line profiles of He II $\lambda 4686$ and He II $\lambda 4859$ are indistinguishable. Note that because the spectra were continuum normalized (§ 2.1), the continuum sections show no significant correlation.

The indication found by MSM of a cyclical, simultaneous modulation of the wind properties and the continuum flux emanating near the stellar core was primarily provided by the inverse correlation existing between the strength of the absorption troughs of N V $\lambda\lambda 4604, 4620$ and the level of continuum flux. The same phenomenon is observed in the present data sets and is quantitatively confirmed by the correlation measurements (e.g., Fig. 7). For *all* epochs, the alternation between filling in and strengthening of these violet absorption edges coincides exactly with maximum and minimum continuum flux, respectively.⁷ For illustration, the gray-scale plot of N V $\lambda\lambda 4604, 4620$ during epoch I

⁶ Note that this appearance of both correlated and anticorrelated variations between the line intensity in some given velocity regions and the continuum flux ensures that it is not an artifact of a systematically (under)overestimated correction of the continuum variability (§ 2.1).

⁷ The phase location of the maximum for epoch IV is dubious because of the severe undersampling of this light curve. Note, however, a maximum at $\phi \sim 0.6-0.7$ in the intensive photometric data gathered about 1 month later by Duijsens et al. (1996).

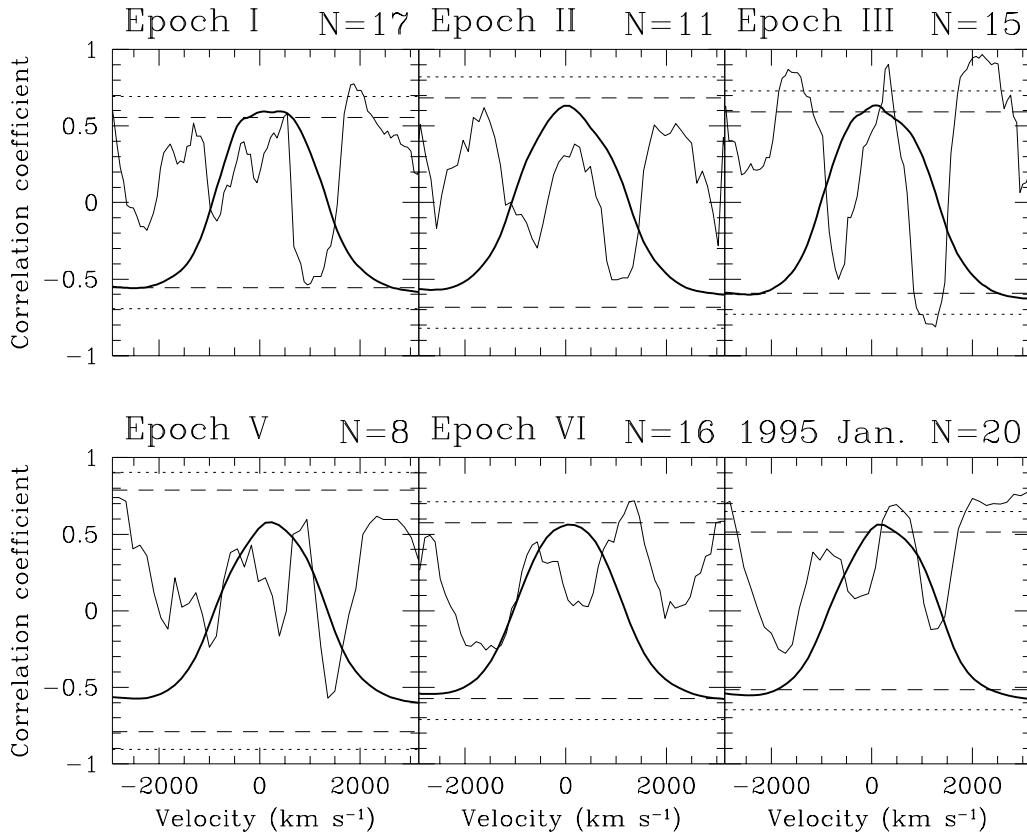


FIG. 6.—Correlation functions of He II $\lambda 4686$ for the different epochs. The epoch and the number of spectra used in this procedure are indicated on the top of each panel. The epoch “1995 Jan” refers to the observations of MSM. The dashed and dotted lines give the 99.0% and 99.9% confidence levels for a significant (anti)correlation, respectively. The mean profile of each epoch is overplotted by a thick line.

is displayed in Figure 8 and can be compared with the continuum light curve of the same epoch in Figure 1 (*top*).

3.4. Temporal Variance Spectrum

As described by MSM, we have calculated the values of the temporal variance spectrum (TVS) (Fullerton et al. 1996), which give a statistical assessment of the variability level at a given wavelength. This quantity (expressed in terms of the typical “size” of the deviations from a template-weighted mean spectrum in percentage of the continuum flux) is shown, along with the 99.0% confidence level for variability, in the lower panels of Figures 4*a–c* and

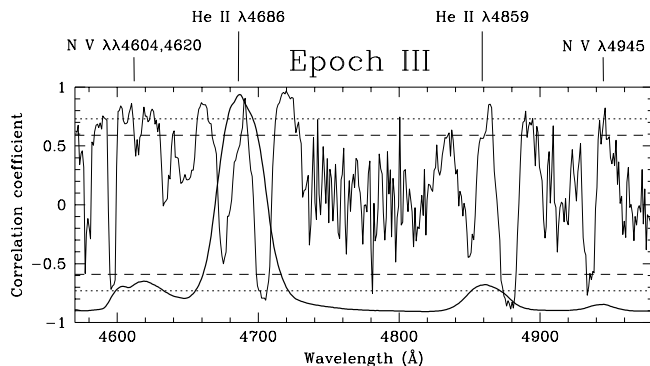


FIG. 7.—Correlation function during epoch III for the spectral domain 4570–4980 Å. The dashed and dotted lines give the 99.0% and 99.9% confidence levels for a significant (anti)correlation, respectively. The mean profile is overplotted by a thick line.

Figure 8. The TVS of He II $\lambda 4686$ and He II $\lambda 4859$ are very similar (Figs. 4*a–b*), highlighting their similar behavior pointed out previously on other grounds (§ 3.2). Significant variations in He II $\lambda 4686$ occur at velocities exceeding the wind-terminal velocity deduced from the bluest saturated point of the UV resonance P Cygni absorption components ($v_\infty \sim 1900 \text{ km s}^{-1}$; Prinja, Barlow, & Howarth 1990).

In Figure 9, we compare the TVS for epochs I, III, and VI and 1995 January for the region encompassing N V $\lambda\lambda 4604, 4620$ and He II $\lambda 4686$ (the number of spectra acquired during the other epochs is too small to yield significant information). It is fairly difficult to assess whether the variability takes place preferentially at the same characteristic velocities from one epoch to another, as recently proposed by Ivanov et al. (1998). Reasons for this are multiple. First, the TVS is particularly sensitive to imperfections in the wavelength calibration (although we tried to minimize this; for more details, see MSM), leading to artificially enhanced variability in the steepest parts of the lines. Second, the reciprocal dispersion of the spectra and phase coverage vary from one epoch to another and can also influence its overall shape. In an effort to assess the influence of the phase coverage on the resultant TVS, we have calculated the TVS for epoch I after rejection of the spectra with $0.0 < \phi < 0.2$, then $0.2 < \phi < 0.4$, and so on. This procedure provided us with five TVSs whose subpeaks are detected in each case to within $\sigma \sim 20 \text{ km s}^{-1}$. In comparison, the subpeaks at ~ -1600 and $\sim +2000 \text{ km s}^{-1}$ in He II $\lambda 4686$ (where the TVS is unaffected by shift of the profile) during epochs I, III, and VI and 1995 January (Fig. 9) present a significantly

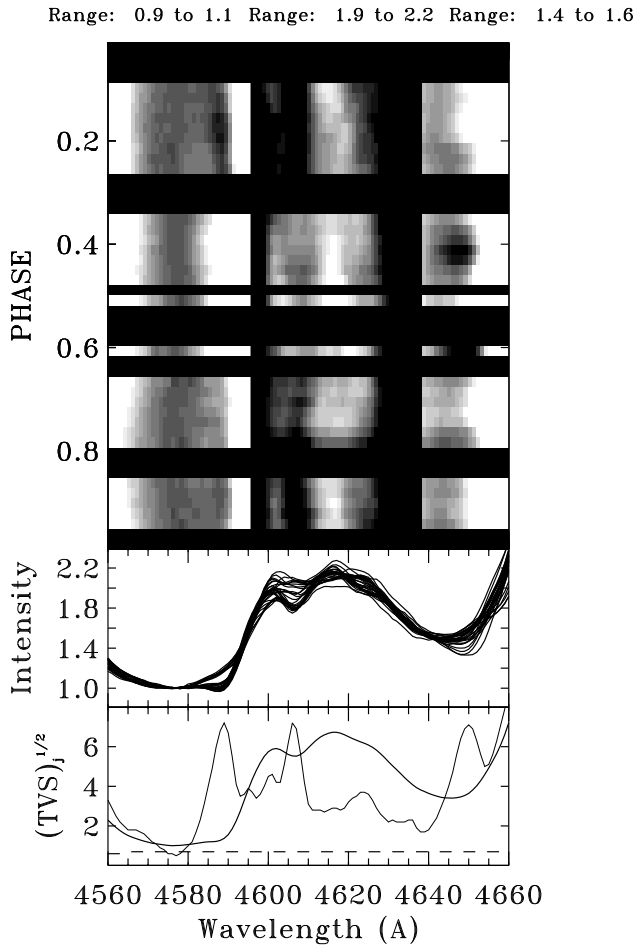


FIG. 8.—Gray-scale plot of the time series of the P Cygni components of N v $\lambda\lambda 4604, 4620$ for epoch I. The selected wavelength domain is displayed for three different intensity intervals. The blue wing variability of He II $\lambda 4686$ is seen at the rightmost panel of this figure.

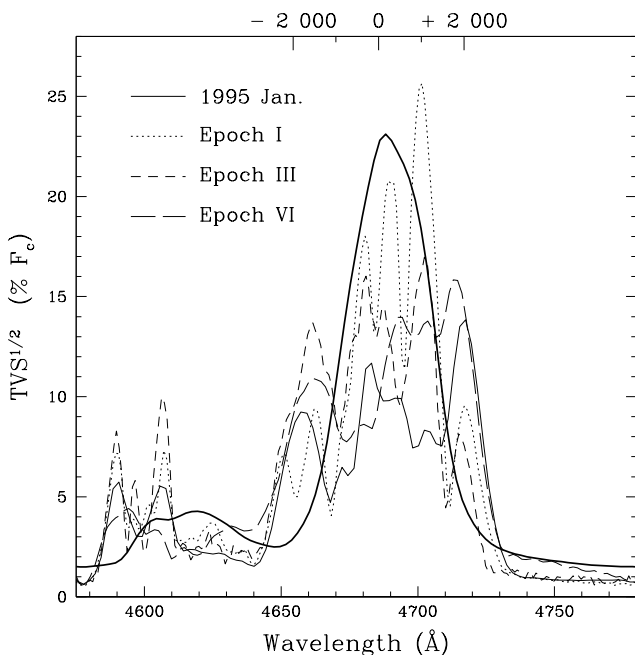


FIG. 9.—Superposition of the TVS of epochs I, III, and VI and 1995 January (MSM) for the spectral domain 4575–4780 Å. A representative mean spectrum is overplotted by a thick line.

higher velocity dispersion: $\sigma \sim 110 \text{ km s}^{-1}$. Therefore, although it would certainly be questionable to draw firm conclusions regarding the long-term behavior of the TVS on the basis of the present data set, preferential variability occurring at significantly different locations across the line profile from one epoch to another is suggested.

3.5. Line Fluxes, FWHM, and Skewness Variations

Figure 10a presents the variations in the line flux of He II $\lambda 4686$ across the wavelength range 4647–4765 Å as a function of phase for each epoch. Note that the plotted variations reflect the net change of emissivity after allowance for the continuum level changes (§ 2.1). MSM found a significant positive correlation between the level of continuum flux and the line flux of this He II transition. However, such a correlation is marginal in this data set for epochs II and VI (compare with Figs. 1 [top] and 2).

Two other quantities, the line skewness and FWHM of He II $\lambda 4686$, are also plotted for the different epochs in Figures 10b–10c, respectively. The skewness gives information on the degree of asymmetry of a given line: zero if it is symmetric, negative or positive if it is skewed longward or shortward in wavelength, respectively. The skewness measurements were restricted to flux levels above two in units of the continuum. A Gaussian fit to the entire profile was applied to determine the FWHMs. Both quantities show evidence for phase-related variations at most epochs. Furthermore, a phase dependence with three relative minima per cycle is suggested for the FWHM variations of epoch I, at $\phi \sim 0.0, 0.4,$ and 0.75 . Relative maxima in skewness appear at these same phases. This is reminiscent of the 1 day recurrence timescale reported in the past, e.g., in the EWs of the UV P Cygni absorption components (Willis et al. 1989; St Louis et al. 1993) or in the optical line-profile FWHM and skewness values (MSM). For the other epochs, however, it is important to note that the situation may be quite different.

4. DISCUSSION

4.1. Implications for the Binary Scenario

In the following discussion, we restrict ourselves to an interpretation of the variability in terms of a single star. The main reason behind this choice is that the possibility of an orbiting low-mass companion as the cause of the 3.77 day variability was discussed in length in MSM and appears to be unlikely. It is of interest, however, to briefly discuss here the implication of these new observations on the binary scenario. In this context, the phase-dependent LPVs presented by N v $\lambda 4945$ are noteworthy (Fig. 4c). If we assume a 3.77 day circular orbit, a canonical mass of the companion of $1.44 M_{\odot}$, and reasonable parameters for EZ CMA ($M_{*} \sim 11.8 M_{\odot}$, $R_{*} = 2.7 R_{\odot}$; Hamann, Koesterke, & Wessolowski 1995), we obtain an orbital separation of $a \sim 9R_{*}$. Since the line-formation region of N v $\lambda 4945$ does not extend beyond $\sim 4R_{*}$ (P. A. Crowther 1995, private communication), it would be difficult to explain how the secondary would significantly perturb these deep layers of the wind via X-ray photoionization, owing in particular to the very high X-ray opacity of the material in this region and the low level of X-ray flux observed (e.g., Stevens & Willis 1988).

4.2. Evidence for a Deep-seated Wind Variability

The analysis of the present data supports a direct link

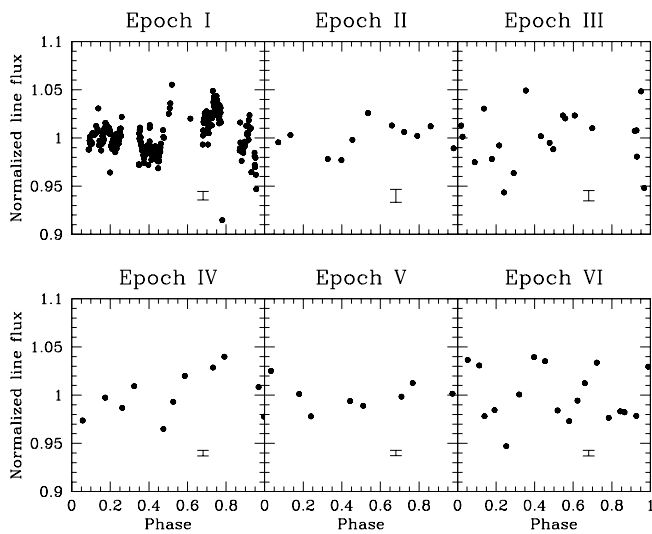


FIG. 10a

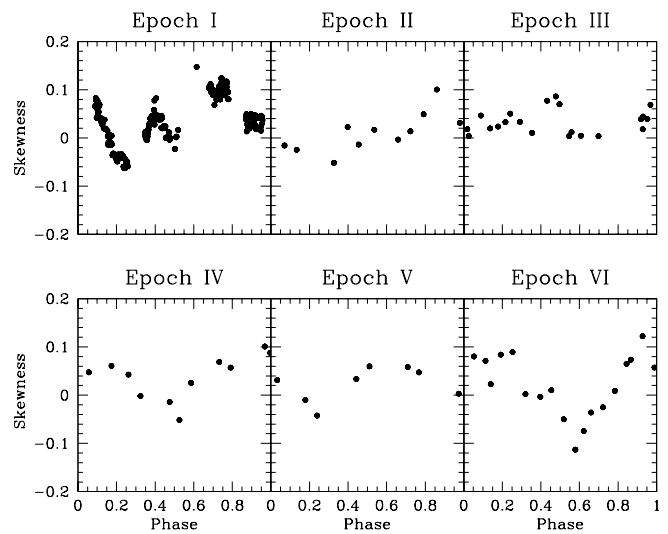


FIG. 10b

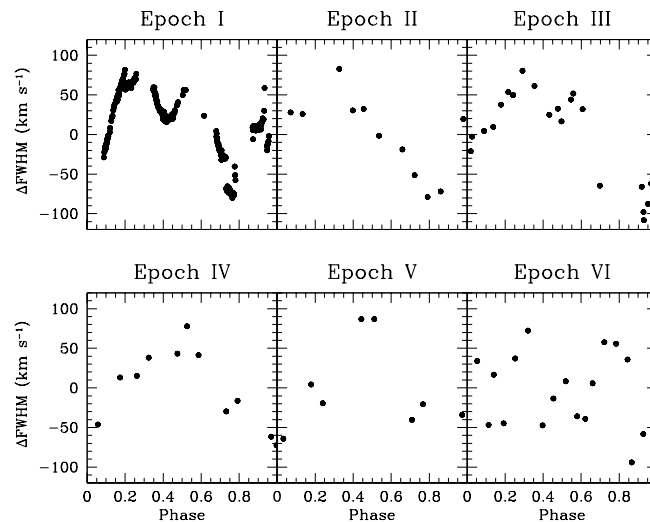


FIG. 10c

FIG. 10.—(a) Line flux of He II $\lambda 4686$ (normalized by division to the mean value in each epoch) as a function of phase. The 2σ error bars were calculated according to Chalabaev & Maillard (1983). Note that they only account for the presence of random noise; they do not allow for possible systematic effects, e.g., imperfect rectification of the spectra. (b) Skewness of He II $\lambda 4686$, as a function of phase, for the six epochs. (c) Deviations of the FWHM for He II $\lambda 4686$ around the mean value (expressed in km s^{-1}), as a function of phase, for the six epochs.

between the line-profile and photometric variations in EZ CMA. Compelling lines of evidence for this are the following. (1) Filling in or strengthening of, for *all* epochs presented here, the violet absorption edge of N V $\lambda 4604$ (and N V $\lambda 4620$), at maximum or minimum continuum flux, respectively (see, e.g., Fig. 8). (2) A significant correlation is occasionally observed between the intensity changes affecting parts of the emission line profiles and the level of continuum flux (e.g., Fig. 6). Although it is not clear why this correlation stands out more clearly at some epochs, it is remarkable in view of the large wind volume sampled by the emission lines, compared to the P Cygni absorption components. (3) The peaks of the correlation function during epoch III (Fig. 6) coincide with the TVS subpeaks for this epoch (Fig. 9), suggesting that the changes in the most variable parts of the profile are directly linked to the variations of the continuum flux.

This often-observed link between the LPVs and the optical continuum flux emanating close to the stellar core

(Hillier 1987) suggests that the wind variability of EZ CMA is rooted to a (azimuthal) spatial dependence of the radiative flux emanating at the base of the outflow. In support of this conclusion, note that the quiescent state of UV spectral variability observed by Willis et al. (1989) was related to a UV continuum flux constant within 0.02 mag.

As demonstrated in the hydrodynamical simulations of Cranmer & Owocki (1996), azimuthal changes in the radiative flux (i.e., driving force) at the very base of an early-type stellar outflow are likely to lead to the formation of wind streams. We propose that this process is operating in EZ CMA. Detailed modeling (beyond the scope of this paper) is required to investigate whether this model is able to account for the observational aspects presented here, notably the correlation observed in Figure 6. Apparently in EZ CMA, as for the B supergiant HD 64760 (Fullerton et al. 1997), there is a strong epoch dependency of the physical conditions at the very base of the outflow, leading to observed wind structure that is different from one epoch to

another. This introduces the epoch-dependent patterns of variability observed (Fig. 3), although the rotation period of the star, which is probably modulating the changes, is always observed.

4.3. *The Cause of a Nonisotropic Base Outflow*

An interesting issue regarding our global understanding of W-R stars is to uncover what underlying physical phenomena operating near (or at) the star's photosphere give rise to the observed wind variations. In this context, pulsations and magnetic structures naturally come to mind.

4.3.1. *Pulsations*

Theoretical investigations of the stability of W-R stars to the ϵ -mechanism (Maeder 1985; Schaller 1991; Cox & Cahn 1988) have shown that the radial fundamental mode is likely to be excited for very deficient hydrogen stars such as EZ CMA (Nugis & Niedzielski 1995). The period of this fundamental mode is predicted to be about 40 minutes for a WNE star. In addition to this, strange-mode instabilities appear in the models of Kiriakidis, Glatzel, & Fricke (1996), with periods of the order 5–10 minutes (Glatzel, Kiriakidis, & Fricke 1993). In contrast, nonradial pulsations are unlikely to prevail in W-R stars (Cox & Cahn 1988; Maeder & Schaller 1991), except perhaps in the objects that are in the H-shell-burning phase (Noels & Scuflaire 1986). From an observational point of view, two objects have been claimed to present periodic photometric variations that could be attributed to pulsational instabilities, namely the two WN8 stars W-R 40 (Blecha, Schaller, & Maeder 1992; but see Martinez et al. 1994) and W-R 66 (Antokhin et al. 1995; Rauw et al. 1996). The *unique* 3.77 day period associated with EZ CMA (Antokhin et al. 1994) seems significantly too long to be associated with pulsations and is more likely to be related to the rotation period. It is, however, important to note that two independent studies found evidence for *transient* rapid (quasi-?) periodic photometric fluctuations (~ 20 minutes) in EZ CMA (Matthews, Moffat, & Marchenko 1992; Bratschi & Blecha 1996). Owing to the unknown nature of the coupling between short-term variations at the very base of the wind such as these *intermittent* variations and the wind conditions, pulsations still cannot be ruled out as driver of the variability. Further investigations are needed to challenge this possibility.

4.3.2. *Magnetic Fields*

Magnetic fields are another possible mechanism that might cause the variability. They can act on the wind either as (1) localized "surface" magnetic features or (2) a large-scale (e.g., dipole or quadrupole) magnetic field probably of fossil origin. One class of objects that have been shown to possess such large-scale magnetic fields are the B-type helium-peculiar stars whose properties are often discussed in the context of the "oblique rotator model" (Shore & Brown 1990). In this model, the magnetic axis is tilted with respect to the rotational axis, leading to a dramatic surface abundance gradient with a subsequent rotational modulation of the spectral lines of these species as different parts of the stellar disk cross the observer's line of sight. The stellar wind is magnetically controlled with the material flowing out freely along the open field lines near the magnetic poles but being trapped at the magnetic equator (Shore 1987). A similar model was recently proposed for the young O7 V star θ^1 Ori C by Stahl et al. (1996).

An overview of the photometric characteristics of EZ CMA (Robert et al. 1992; Duijsens et al. 1996; MSM) leads to the conclusion that the observed practically *continuous* changes in the light curve morphology (see Marchenko & Moffat 1998) could fit naturally into a picture where extended magnetic regions on the stellar core experience changes in their activity on a monthly timescale. Moreover, the long-term (~ 6.6 yr) variability in the star's luminosity hinted at by the data of Duijsens et al. (1996) could be related to cyclic magnetic activity (see, e.g., Baliunas & Vaughan 1985). Finally, possible flares in EZ CMA have been independently reported by Matthews et al. (1992a) and Duijsens et al. (1996).

However, there exists a fundamental difficulty related to the generation of such a magnetic activity. Although Schaefer (1996) found evidence in his evolutionary models for a small convective zone close to the surface of WNL stars, W-R stars are believed to lack the outer and extended convective zone required for the creation of a dynamo-generated magnetic field. At present, there are no satisfactory alternatives to account for the putative formation of photospheric magnetic structures in W-R stars. A more complete description of the internal structure of these objects is required to address this issue. This problem is somewhat reminiscent of the Herbig Ae/Be stars, for which alternative mechanisms for the creation of a corona have been invoked in order to account for their X-ray and LPV properties (Tout & Pringle 1995).

Thus, some preference should perhaps be given to the existence of a large-scale, fossil corotating magnetic structure because it is less dependent on a mechanism to create and sustain magnetic activity in the envelope of EZ CMA. Although global fields have been proposed in order to explain the (very similar to EZ CMA) epoch-dependent photometric variations presented by some Be stars (Balona, Sterken, & Manfroid 1991), the major drawback of this model is that it cannot easily account for the long-term changes observed. If confirmed by more intensive time-resolved X-ray observations, the lack of phase-locked variability suggested by the *ROSAT* data (Willis & Stevens 1996) would challenge the relevance of the oblique rotator model to EZ CMA (see Gagné et al. 1997; Babel & Montmerle 1997).

Finally, it is not clear whether the inconclusive searches for magnetic fields in EZ CMA conducted so far (see the circular polarization observations of McLean et al. 1979 in low-resolution spectral mode; Drissen et al. 1989; Robert et al. 1992) are telling or are due, for instance, to orientation effects (Barker et al. 1981) or other constraints (e.g., lack of sufficient spectral resolution or sensitivity to weak fields). Polarimetric and radio observations of O stars (which are the precursors of W-R stars) put generous upper limits of some hundred gauss on the strength of any large-scale ordered fields (Bohlender 1994; Bieging, Abbott, & Churchwell 1989). If the same field limits apply also to EZ CMA, their detection would be extremely difficult even with present state-of-the-art polarimetric techniques. A more promising avenue might be via the detection of the Hanle effect in UV lines (Ignace, Nordsieck, & Cassinelli 1997).

We would like to thank D. Fortier and B. Sanscartier for their help in the reduction procedure. We acknowledge I. Antokhin and D. Duijsens for their permission to reproduce Figures 1 (*top*) and 1 (*bottom*), respectively. We

thank S. V. Marchenko for a careful reading of this manuscript. T. M., N. S. L., A. F. J. M., and G. M. H. wish to thank the Natural Sciences and Engineering Research

Concil (NSERC) of Canada and the Fonds pour la Formation de Chercheurs et l'Aide à la Recherche (FCAR) of Québec for financial support.

REFERENCES

- Antokhin, I., Bertrand, J.-F., Lamontagne, R., & Moffat, A. F. J. 1994, *AJ*, 107, 2179
- Antokhin, I., Bertrand, J.-F., Lamontagne, R., Moffat, A. F. J., & Matthews, J. 1995, *AJ*, 109, 817
- Babel, J., & Montmerle, T. 1997, *ApJ*, 485, L29
- Baliunas, S. L., & Vaughan, A. H. 1985, *ARA&A*, 23, 379
- Balona, L. A., Sterken, C., & Manfroid, J. 1991, *MNRAS*, 252, 93
- Barker, P. K., Landstreet, J. D., Marlborough, J. M., Thompson, I., & Maza, J. 1981, *ApJ*, 250, 300
- Biegging, J. H., Abbott, D. C., & Churchwell, E. B. 1989, *ApJ*, 340, 518
- Blecha, A., Schaller, G., & Maeder, A. 1992, *Nature*, 360, 320
- Bohlender, D. A. 1994, in *IAU Symp.* 162, Pulsation, Rotation and Mass Loss in Early-Type Stars, ed. L. A. Balona, H. F. Henrichs, & J. M. LeContel (Kluwer: Dordrecht), 155
- Bratschi, P., & Blecha, A. 1996, *A&A*, 313, 537
- Cardona, O., St-Louis, N., Koenigsberger, G., Vazquez, G. A., Piceno, G., Moffat, A. F. J., Georgiev, L., & Ivanov, M. 1998, in preparation
- Chalabaev, A., & Maillard, J. P. 1983, *A&A*, 127, 279
- Cox, A. N., & Cahn, J. H. 1988, *ApJ*, 326, 804
- Cranmer, S. R., & Owocki, S. P. 1996, *ApJ*, 462, 469
- Drissen, L., Robert, C., Lamontagne, R., Moffat, A. F. J., St-Louis, N., van Weeren, N., & van Genderen, A. M. 1989, *ApJ*, 343, 426
- Duijnsens, M. F. J., van der Hucht, K. A., van Genderen, A. M., Schwarz, H. E., Linders, H. P. J., & Kolkman, O. M. 1996, *A&AS*, 119, 37
- Ebbets, D. 1979, *PASP*, 91, 804
- . 1982, *ApJS*, 48, 399
- Eversberg, T., Lépine, S., & Moffat, A. F. J. 1998, *ApJ*, 494, 799
- Firmann, C., Koenigsberger, G., Bisiacchi, G. F., Moffat, A. F. J., & Isserstedt, J. 1980, *ApJ*, 239, 607
- Fullerton, A. W., Gies, D. R., & Bolton, C. T. 1996, *ApJS*, 103, 475
- Fullerton, A. W., Massa, D. L., Prinja, R. K., Owocki, S. P., & Cranmer, S. R. 1997, *A&A*, 327, 699
- Gagné, M., Caillault, J.-P., Stauffer, J. R., & Linsky, J. L. 1997, *ApJ*, 478, L87
- Georgiev, L. N., & Ivanov, M. M. 1995, in *IAU Symp.* 163, Wolf-Rayet Stars: Binaries, Colliding Winds, Evolution, ed. K. A. van der Hucht & P. M. Williams (Dordrecht: Kluwer), 54
- Glatzel, W., Kiriakidis, M., & Fricke, K. J. 1993, *MNRAS*, 262, L7
- Gosling, J. T. 1996, *ARA&A*, 34, 35
- Grady, C. A., Snow, T. P., & Timothy, J. G. 1983, *ApJ*, 271, 691
- Hamann, W.-R., Koesterke, L., & Wessolowski, U. 1995, *A&A*, 295, 151
- Harmanec, P. 1991, in *ESO Workshop on Rapid Variability of OB-Stars: Nature and Diagnostic Value*, ed. D. Baade (Garching: ESO), 265
- Harries, T. J., Hillier, D. J., & Howarth, I. D. 1998, *MNRAS*, in press
- Hillier, D. J. 1987, *ApJS*, 63, 947
- Howarth, I. D., Prinja, R. K., & Massa, D. 1995, *ApJ*, 452, L65
- Hundhausen, A. J. 1972, *Coronal Expansion and Solar Wind* (Berlin: Springer)
- Ignace, R., Nordsieck, K. H., & Cassinelli, J. P. 1997, *ApJ*, 486, 550
- Ivanov, M. M., Georgiev, L. N., Koenigsberger, G., & Valchev, T. S. 1998, *A&A*, submitted
- Kaper, L., Henrichs, H. F., Nichols, J. S., Snoek, L. C., Volten, H., & Zwarthoed, G. A. A. 1996, *A&AS*, 116, 257
- Kaper, L., et al. 1997, *A&A*, 327, 281
- Kaufer, A., Stahl, O., Wolf, B., Gäng, Th., Gummersbach, C. A., Kovács, J., Mandel, H., & Szeifert, Th. 1996a, *A&A*, 305, 887
- Kaufer, A., et al. 1996b, *A&A*, 314, 599
- Kiriakidis, M., Glatzel, W., & Fricke, K. J. 1996, *MNRAS*, 281, 406
- Koenigsberger, G. 1995, in *IAU Symp.* 163, Wolf-Rayet Stars: Binaries, Colliding Winds, Evolution, ed. K. A. van der Hucht & P. M. Williams (Dordrecht: Kluwer), 538
- Lamontagne, R., Moffat, A. F. J., & Lamarre, A. 1986, *AJ*, 91, 925
- Lépine, S., Moffat, A. F. J., & Henriksen, R. N. 1996, *ApJ*, 466, 392
- Maeder, A. 1985, *A&A*, 147, 300
- Maeder, A., & Schaller, G. 1991, in *IAU Symp.* 143, Wolf-Rayet Stars and Interrelations with Other Massive Stars in Galaxies, ed. K. A. van der Hucht & B. Hidayat (Dordrecht: Kluwer), 167
- Marchenko, S. V., & Moffat, A. F. J. 1998, *ApJ*, submitted
- Marchenko, S. V., Moffat, A. F. J., Eversberg, T., Hill, G. M., Tovmassian, G., Morel, T., & Seggewiss, W. 1998, *MNRAS*, in press
- Martinez, P., Kurtz, D., Ashley, R., & Tripe, P. 1994, *Nature*, 367, 601
- Massa, D., Prinja, R. K., & Fullerton, A. W. 1995, *ApJ*, 452, 842
- Matthews, J. M., Moffat, A. F. J., & Marchenko, S. V. 1992a, *A&A*, 266, 409
- Matthews, J. M., St-Louis, N., Moffat, A. F. J., Drissen, L., Koenigsberger, G., Cardona, O., & Niemela, V. S. 1992b, in *ASP Conf. Proc.* 22, Non-isotropic and Variable Outflows from Stars, ed. L. Drissen, C. Leitherer, & A. Nota (San Francisco: ASP), 130
- McLean, I. S., Coyne, G. V., Frecker, J. E., & Serkowski, K. 1979, *ApJ*, 231, L141
- Moffat, A. F. J., & Robert, C. 1992, in *ASP Conf. Proc.* 22, Nonisotropic and Variable Outflows from Stars, ed. L. Drissen, C. Leitherer, & A. Nota (San Francisco: ASP), 203
- Morel, T., St-Louis, N., & Marchenko, S. V. 1997, *ApJ*, 482, 470 (MSM)
- Mullan, D. J. 1984, *ApJ*, 283, 303
- . 1986, *A&A*, 165, 157
- Noels, A., & Scuflaire, R. 1986, *A&A*, 161, 125
- Nugis, T., & Niedzielski, A. 1995, *A&A*, 300, 237
- Owocki, S. P., Cranmer, S. R., & Fullerton, A. W. 1995, *ApJ*, 453, L37
- Press, W. H., Teukolsky, S. A., Vetterling, W. T., & Flannery, B. P. 1992, *Numerical Recipes* (Cambridge: Cambridge Univ. Press), 634
- Prinja, R. K., Barlow, M. J., & Howarth, I. D. 1990, *ApJ*, 361, 607
- Prinja, R. K., & Fullerton, A. W. 1994, *ApJ*, 426, 345
- Prinja, R. K., Fullerton, A. W., & Crowther, P. A. 1996, *A&A*, 311, 264
- Prinja, R. K., Massa, D., & Fullerton, A. W. 1995, *ApJ*, 452, L61
- Rauw, G., Gosset, E., Manfroid, J., Vreux, J.-M., & Claeskens, J.-F. 1996, *A&A*, 306, 783
- Reid, A. H. N., & Howarth, I. D. 1996, *A&A*, 311, 616
- Robert, C., et al. 1992, *ApJ*, 397, 277
- Schaerer, D. 1996, *A&A*, 309, 129
- Schaller, G. 1991, in *ASP Conf. Proc.* 11, Confrontation Between Stellar Pulsation and Evolution, ed. C. Cacciati & G. Clementini (San Francisco: ASP), 304
- Schulte-Ladbeck, R. E. 1995, in *IAU Symp.* 163, Wolf-Rayet Stars: Binaries, Colliding Winds, Evolution, ed. K. A. van der Hucht & P. M. Williams (Dordrecht: Kluwer), 176
- Schulte-Ladbeck, R. E., Nordsieck, K. H., Taylor, M., Bjorkman, K. S., Magalhães, A. M., & Wolff, M. J. 1992, *ApJ*, 387, 347
- Shore, S. N. 1987, *AJ*, 94, 731
- Shore, S. N., & Brown, D. N. 1990, *ApJ*, 365, 665
- Smith, L. F., Shara, M. M., & Moffat, A. F. J. 1996, *MNRAS*, 281, 163
- Stahl, O., et al. 1996, *A&A*, 312, 539
- Stevens, I. R., & Willis, A. J. 1988, *MNRAS*, 234, 783
- St-Louis, N. 1994, *Ap&SS*, 221, 197
- St-Louis, N., Dalton, M. J., Howarth, I. D., Willis, A. J., & Conti, P. S. 1998, in preparation
- St-Louis, N., Dalton, M. J., Marchenko, S. V., Moffat, A. F. J., & Willis, A. J. 1995, *ApJ*, 452, L57
- St-Louis, N., Howarth, I. D., Willis, A. J., Stickland, D. J., Smith, L. J., Conti, P. S., & Garmany, C. D. 1993, *A&A*, 267, 447
- Strassmeier, K. G., & Hall, D. S. 1988, *ApJS*, 67, 439
- Tout, C. A., & Pringle, J. E. 1995, *MNRAS*, 272, 528
- Willis, A. J., Howarth, I. D., Smith, L. J., Garmany, C. D., & Conti, P. S. 1989, *A&AS*, 77, 269
- Willis, A. J., & Stevens, I. R. 1996, *A&A*, 310, 577
- Young, A. T., et al. 1991, *PASP*, 103, 221